An Overview of the SmartSuit Architecture

Logan Kluis[1], Nathan Keller[2],
Texas A&M University, College Station, TX, 77840, USA

Narahari Iyengar[3], Hedan Bai[4], Robert Shepherd[5],
Cornell University, Ithaca, NY, 14853, USA,

and

Ana Diaz-Artiles[6]
Texas A&M University, College Station, TX, 77840, USA

SmartSuit is an advanced planetary spacesuit for the next generation of exploration missions that capitalizes on a novel architecture to improve on current gas-pressurized spacesuits. The SmartSuit, while gas-pressurized, also incorporates the following three technological innovations: 1) a full-body soft-robotic layer inside the gas-pressurized suit to enhance mobility, 2) an outer layer made of stretchable self-healing skin to enhance safety, 3) stretchable optoelectronic sensors embedded in the membrane to improve interaction with the environment and monitor skin membrane integrity. SmartSuit will exploit soft-robotic actuation to counteract spacesuit joint torques, thus improving mobility and metabolic expenditure on EVA missions. Additionally, the soft-robotic layer also provides mechanical counterpressure (MCP) to the wearer, which allows a decrease in the gas-operating pressure within the suit (therefore further enhancing suit mobility), and/or relaxing prebreathe requirements. We expect the proposed spacesuit soft-robotic technology to also reduce the numerous spacesuit-fit injuries and discomfort experienced by present astronauts due to the current highly pressurized spacesuits with no robotic assistance. In this paper, we introduce our SmartSuit spacesuit architecture and present preliminary results on feasibility and prototyping, and we discuss potential benefits during future planetary exploration missions. In particular, we built and characterized two knee soft-robotic actuator prototypes in the context of the SmartSuit, and we compared theoretical and empirical performance limits. Additionally, we conducted a human-spacesuit biomechanics analysis and quantified improvements in metabolic expenditures and other biomechanical metrics from the soft-robotic actuators. Finally, we present prototype testing of the self-healing membrane and performance of the optoelectronic sensors. These features of the SmartSuit were considered in the current mission architecture for EVAs on the Mars Design Reference Mission 5.0.

Nomenclature

DCS	=	decompression sickness
EMU	=	extravehicular mobility unit
EVA	=	extravehicular activity
ISS	=	International Space Station
MCP	=	mechanical counterpressure
PSID	=	pounds per square inch differential
sPUU	=	self-healing polyurethane urea

[1] Graduate Researcher, Department of Aerospace Engineering, 701 H.R. Bright Building 3141, Rm 203
[2] Graduate Researcher, Department of Health and Kinesiology, 701 H.R. Bright Building 3141, Rm 203
[3] Graduate Researcher, Sibley School of Mechanical and Aerospace Engineering, 130 Upson Hall
[4] Graduate Researcher, Sibley School of Mechanical and Aerospace Engineering, 130 Upson Hall
[5] Associate Professor, Sibley School of Mechanical and Aerospace Engineering, 130 Upson Hall
[6] Assistant Professor, Department of Aerospace Engineering, 701 H.R. Bright Building 3141, Rm 620B

I. Introduction

Current extravehicular activities (EVAs) aboard the International Space Station (ISS) are performed using the extravehicular mobility unit (EMU) spacesuit, which is pressurized to 4.3 psia (29.6 kPa) at 100% oxygen.[1] A combination of the gas-pressurization and poor fit inside the EMU has resulted in a spacesuit environment that is injury prone,[2–13] energy inefficient,[14–17] and impairs movement.[18–23] Astronauts on future planetary EVA missions will operate in the exploration extravehicular mobility unit (xEMU), which is also gas-pressurized and capable of pressurizing to 8.2 psia (56.5 kPa).[24] Built for movement on planetary surfaces, the mobility of the xEMU will be an improvement on the EMU, but high operating pressures may exacerbate existing problems of the EMU and lead to poor performance in EVAs that already bear many risks.[25]

In this context, we propose SmartSuit, a novel spacesuit architecture for EVA on Mars and other planetary surfaces that increases human performance for the next generation of exploration missions. SmartSuit introduces soft-robotic technology into the spacesuit, improving mobility by allowing for a fuller range of movements while performing an EVA. Additionally, the mechanical counterpressure (MCP) generated by the soft-robotic layer inside the suit reduces pre-breathe times, which currently can last up to four hours[26–29] and therefore, entail a large investment of mission resources (i.e., astronaut time). The spacesuit also incorporates a soft and stretchable self-healing membrane located in the outer layer that not only protects the astronaut, but also collects data through transparent sensors embedded in the self-healing membrane. Surface displacements are more efficient, and the optoelectronic technology embedded in the membrane allows for an enhanced interaction with the environment during EVA traverses, and permits astronauts to interact with and "feel" rocks directly during a sampling traverse when exploring the Martian surface. This enhanced interaction during traverses also enables greater crew autonomy and facilitates *in-situ* decision making. In summary, EVA times can be drastically reduced through all phases of EVA: pre-breathe time, transportation to worksite, and worksite operations. The SmartSuit concept and technologies are summarized in Figure 1. In the present publication, we review the SmartSuit architecture, present the results of our initial investigations and prototyping, and discuss future benefits of the technological innovations.

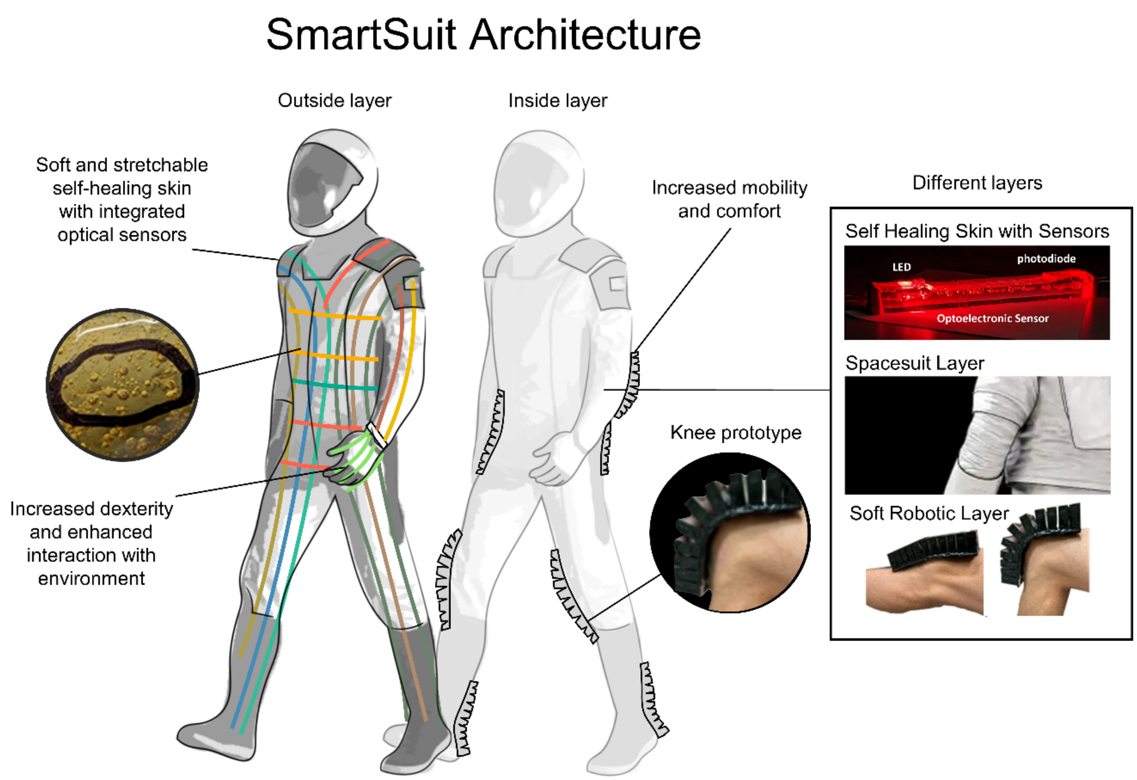

Figure 1. SmartSuit spacesuit architecture, which features three technological innovations: 1) a full-body soft-robotic layer inside the gas-pressurized spacesuit to enhance mobility, 2) an outer layer made of stretchable self-healing skin to enhance safety, and 3) stretchable integrated optoelectronic sensors embedded in the membrane to enhance interaction with the environment and monitor skin membrane integrity. (Credit figure: Pat Pataranutaporn)

II. Soft-Robotic Elements

A. Introduction to Soft-Robotics to Enhance Human Performance

We propose the use of soft-robotic elements to improve human-spacesuit interaction and mitigate the adverse effects of assistive devices made of hard materials. Robotic elements, such as exoskeletons, could greatly enhance human performance during planetary exploration. However, exoskeletons comprised of hard materials can cause contact injuries and abnormal gait patterns,[30] and their integration into spacesuits is difficult.[31] Soft-robotic actuation will allow astronauts to use their full range of motion at a fraction of the effort previously needed without robotic assistance, and without the additional pain and discomfort of hard elements. Soft-robotic elements have been previously used on robotic gloves.[32] Each finger had a series of interconnected chambers that could expand upon pressurization, resulting in a grasping motion, and allowing the soft-robotic glove to improving grip strength by 60%.[32] Using conventional composite beam theory for actuator motion analysis, the maximum net moment produced by a finger is:

$$M_{max} = \pi * r^3 * \Delta p \qquad (1)$$

where r is the radius of the glove chamber of the aforementioned finger when pressurized and Δp is the applied pressure differential. This equation indicates that an increasing pressure differential or height of the pressure chambers in the actuator increase the maximum theoretical torque that can be produced.

B. Design and Testing of Soft-Robotic Knee Prototypes

For our specific application to the spacesuit, we designed and built two soft-robotic knee actuator prototypes (Figure 2). Both models are made of carbon resin – elastic polyurethane (EPU40, Carbon 3D Incorporated) and manufactured by combining 3D printing and bonding techniques (Digital Light Synthesis, DLS). These models were specifically made for the knee, but we envision to incorporate the same technology in other joints used for ambulation. The first prototype has a series of interconnected air chambers and a strain-limiting layer along the knee side, so upon fluid pressurization, the actuator causes a bending motion.

The second prototype #2 was made such that the actuator lacks a strain limiting layer, which would be replaced by the wearer's knee. This design requires the hollow chambers to be connected by stretchable external tubing, as can be seen in Figure 2. Upon fluid pressurization, the chambers inflate and push against each other.

Prototype #1 **Prototype #2**

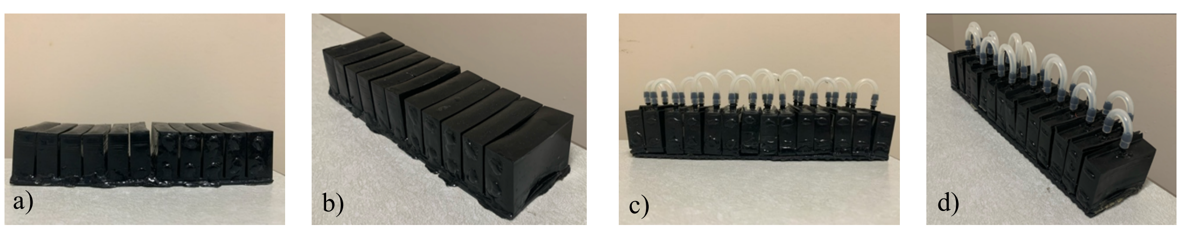

Figure 2. Knee soft-robotic prototype #1 with integrated strain-limiting layer (chambers are connected internally through the strain-limiting layer): front view (a) and isometric view (b). Knee soft-robotic prototype #2 without integrated strain-limiting layer (chambers are connected via external stretchable tubing and extendable layer than allows elongation in the axial direction): front view (c) and isometric view (d).

To characterize the performance of the actuators, a test bed was created to conduct a four-point bending test (shown in Figure 3) and characterize the relationships between pressurization differential (psid), bending angle (degrees), and torque produced (Nm). During testing, a known force F was applied on the actuators using two cables located at known distances D from the edges of the testing apparatus, and the actuator was pressurized at increasing increments. Based on conventional beam theory and under these circumstances, the maximum moment (M) generated by an actuator under a pre-defined force F is defined by:

$$M = \frac{1}{2} DF \qquad (2)$$

For prototype #1, testing pressures ranged from 1 to 15 psid (103 kPa). The pressure differential limit of 15 psid (103 kPa) was set due to safety considerations given that this was the first prototype iteration and the relatively simple design of our test bed. For prototype #2, improved manufacturing permitted a pressure differential of 20 psid (138 kPa). Additionally, blue markers were positioned at known locations to facilitate the calculation of the bending angle at each testing condition. Thus, images of the loaded and pressurized actuator were taken at each test condition and were later analyzed by a custom script to calculate the bending angle of the actuator. The angle was limited to a maximum of approximately 85 degrees due to the actuator folding back on itself. Figure 3 shows the process of calculating the bending angle based on the blue markers identified on the actuator.

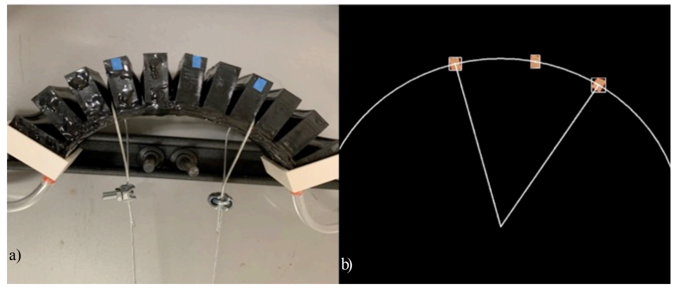

Figure 3. Images of the prototype #1 loaded with known forces and pressurized during four-point bending testing. The actuator also has three blue markers that were used to calculate the bending angle generated during each test condition (a); Screenshot of the script created to calculate the bending angle based on the three blue marker positions (b).

Results are illustrated in Figure 4 where the full range of pressures, angles, and torques generated are shown for both actuators. Prototype #1 was capable of reaching a torque of 4.6 Nm with a pressurization of 15 psid at an angle of approximately 24 degrees. Theoretically, we can calculate the expected assistive-net moment generated by the new actuator design using Equation (1): using a fluid pneumatic pressure equal to Δp = 15 psid (103 kPa), and a radius of r = 2.5 cm, the theoretical maximum soft-robotic induced moment yields $M_{N_{max}} = 5.1\ Nm$. Thus, the maximum torque generated experimentally was approximately 9% smaller than the ideal maximum torque.

Using the same four-point bending methodology, prototype #2 was capable of producing 10.7 Nm at an angle of 26 degrees when pressurized at 20 psid (138 kPa). Theoretically, using a pressure of Δp = 20 psid (138 kPa) and a knee radius (simulated with an artificial restrained layer) of r = 3 cm, the maximum soft-robotic induced moment yields $M_{N_{max}} = 11.7\ Nm$, which is close to what we were able to achieve experimentally. This value is also higher than the maximum EMU induced knee torque during walking (~10 Nm). Actuator performance and functional testing on a human subject still needs to be proven, including an investigation on how to better accommodate and fix the actuator onto a body joint such as the knee.

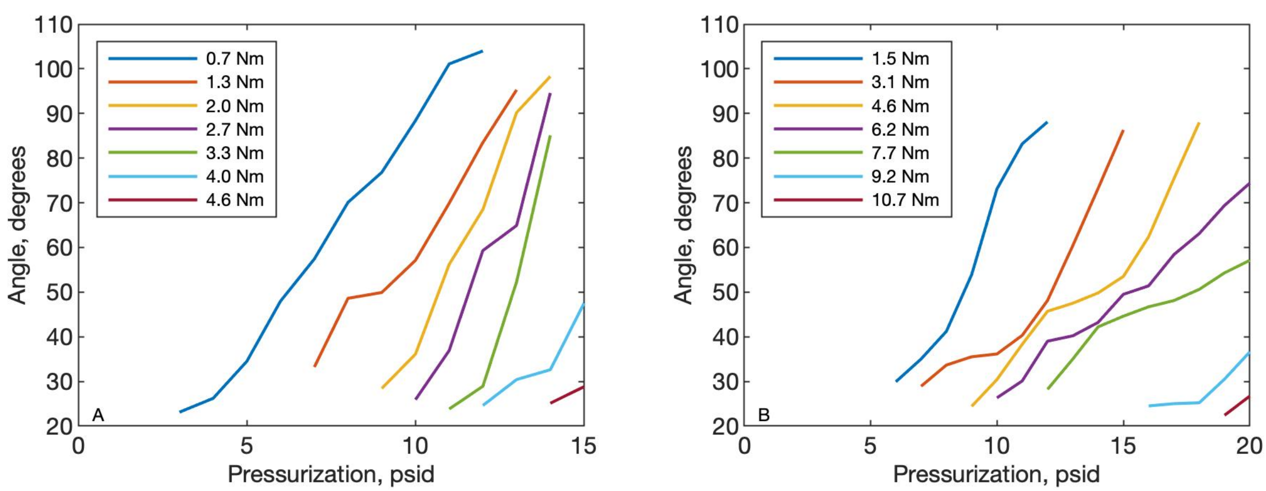

Figure 4. Relationships between bending angle generated, pressurization applied to actuate, and torque produced by the actuator prototype #1 (a) and Prototype #2 (b). The higher the moment, the larger the pressure necessary to create the same angle. Alternatively, a larger torque for a given angle requires a higher pressure. The maximum torque generated by prototype #1 was ~4.6 Nm at 15 psid. The maximum torque generated by prototype #2 was ~10.7 Nm at 20 psid.

C. Reduction of Spacesuit Joint Torques – Biomechanical Analysis

To study to the impact of our soft-robotic actuators on spacesuit performance, we developed a computational framework[33,34] using OpenSim.[35] OpenSim is a biomechanics software that is capable of computing inverse kinematics, inverse dynamics, and computed muscle control for motions such as walking[36] and running.[37] Utilizing joint torques obtained from experimental spacesuit testing,[20,38,39] the metabolic rate of walking with applied spacesuit joint torques can also be calculated.[40,41] We used this framework to investigate motion biomechanics and metabolic cost of a walking motion in unsuited conditions (Unsuited), in EMU-suited conditions (EMU), and in EMU-suited conditions with assistive actuators incorporated in the SmartSuit soft-robotic layer (EMU-assisted) (see Figure 5). In our simulations, we used a 3D musculoskeletal model with 54 linear muscle actuators and 23 degrees of freedom[42], representing an astronaut model of 75 kg and 1.8 m of height.

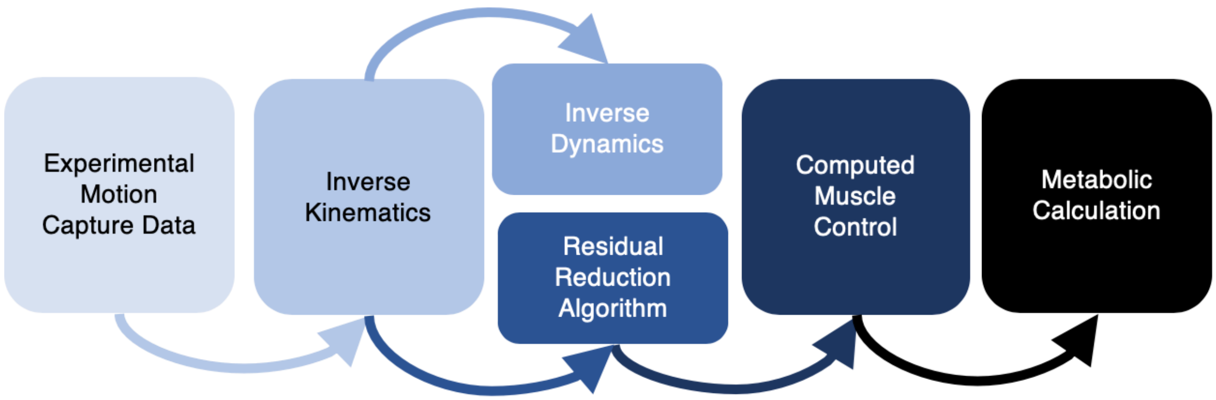

Figure 5. The summarized OpenSim methodology implemented for our biomechanical simulations. Experimental motion capture data refers to the data recorded from experiments (we used existing walking data available through OpenSim). Inverse Kinematics computes the joint position and angles of the musculoskeletal model. Inverse Dynamics solves for the forces and torques of the model's joints and segments. Using the Residual Reduction Algorithm, we are able to minimize errors in the joints and body locations. Finally, individual muscle force and soft-robotic actuator activation are calculated using Computed Muscle Control, which can then be used to determine the metabolic cost of the simulation.

For the suited simulations, external EMU torques from the ankle, knee, and hip were applied to the musculoskeletal model, and an example of the knee torques is shown in Figure 6. Figure 6A shows the angle-joint torque relationships of the EMU spacesuit. Figure 6B presents the knee angle (i.e., kinematics) of our model throughout one gait cycle of the walking simulation. Finally, based on Figure 6A and Figure 6B, Figure 6C shows the resulting applied joint torque to the model during the particular walking motion being analyzed. Taken together, for example, we can see that at 50% of the gait cycle, Figure 6B shows the left knee is at approximately 60 degrees and performing an extension motion because the joint angle is decreasing. Figure 6A indicates that the applied joint torque at 60 degrees in extension is a negative 5 Nm torque (resisting knee extension) and this is confirmed in Figure 6C. The sudden changes in applied torque (e.g., right knee at ~70% of gait cycle) can be attributed to the knee joint changing its direction of motion (e.g., flexion to extension). The rest of joint angles and applied joint torques can be found elsewhere.[34]

In addition to the EMU simulations (EMU conditions), another set of simulations was completed in which robotic actuators at the hip, knee, and ankle joints assisted in ambulation (EMU-assisted). We investigated the following maximum torque limits for the actuators: 5 Nm, 10 Nm, and 15 Nm. These three limits were chosen for several reasons. First, a torque of 5 Nm is capable of being produced by the 2nd prototype actuator at all joint angles achieved by the ankle, knee, and hip (Figure 6). For example, the highest angle achieved in the knee is approximately 70 degrees, at which the 2nd prototype actuator can produce 6.2 Nm of torque when pressurized to 19 psid (131 kPa). Second, 10 Nm is approximately the limit of torque produced by the 2nd prototype when pressurized to the 20 psid (138 kPa) limit. Unlike the 5 Nm limit, the actuator can only sustain the 10 Nm of torque up to 23 degrees. Finally, 15 Nm is used as a reference for future iterations of the soft-robotic actuator that may produce higher amounts of torque. Thus, using a metabolic model developed and improved by Umberger[40,41] and the methodology characterized by our previous publications,[33,34] we calculated the metabolic cost of walking without spacesuit joint torques (Unsuited), with EMU join torques (EMU), and with EMU joint torques and soft-robotic actuators at various actuator limits (EMU-assisted).

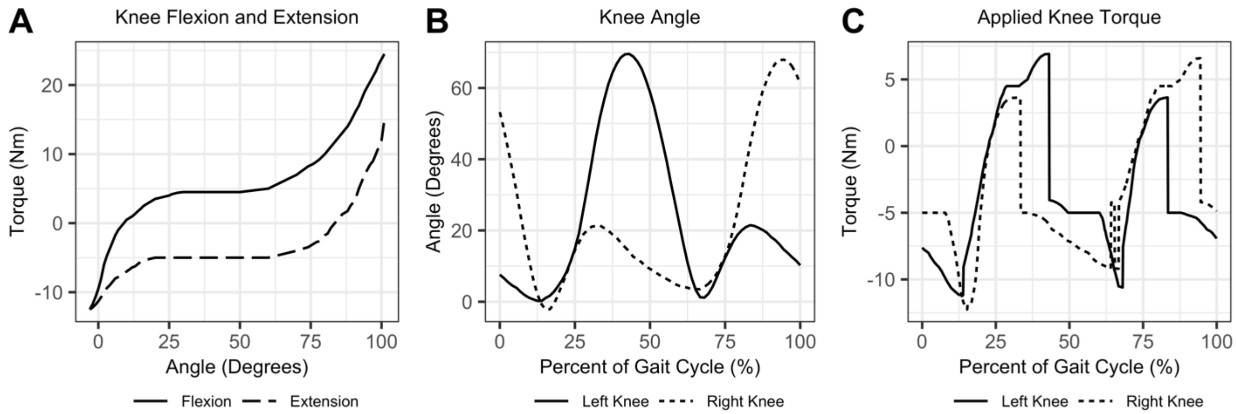

Figure 6. A) EMU knee joint-torque relationship (flexion/extension), B) knee kinematics of the musculoskeletal model throughout one gait cycle of the walking simulation (0 degrees represents the tibia parallel with the femur, flexion is positive), C) associated EMU knee joint-torques applied to the musculoskeletal model throughout one gait cycle of the walking simulation (positive torques resist knee flexion). A similar process is also performed for the ankle and hip joints. See full results.[34] Adapted from.[18,38]

Table 1 describes the results from our simulations. The metabolic cost is shown in terms of Kilocalories/Gait Cycle and Kilocalories/Hour for Unsuited, EMU, and EMU-assisted conditions at various assistive actuator conditions. The second column specifies energy expenditure in terms of one gait cycle (right heel strike to right heel strike) and the third column specifies energy cost in terms of time (approximately 1 gait cycle every 1.2 seconds). Our results indicate that the addition of 5, 10, and 15 Nm of soft-robotic actuation could improve spacesuit ambulation by up to 33, 144, and 227 kilocalories/hour respectively. Soft-robotic actuators that produced 5 Nm of torque have a minor impact on the metabolic performance while incremental additions of 5 Nm significantly increase performance of spacesuit ambulation. These results indicate that a soft-robotic actuator that is capable of producing 15 Nm of torque up to 70 degrees is an excellent goal for future iterations of our actuator design.

Table 1. Total metabolic cost for Unsuited, EMU, and EMU-assisted walking conditions. The addition of 5, 10, and 15 Nm of soft-robotic actuation to the EMU improves metabolic performance by 33, 144, and 227 kilocalories/hour respectively.

Condition	Kilocalories/Gait Cycle	Kilocalories/Hour
Unsuited	0.170	510
EMU	0.315	943
EMU-assisted (5 Nm Actuators)	0.305	910
EMU-assisted (10 Nm Actuators)	0.267	799
EMU-assisted (15 Nm Actuators)	0.240	716

We used an already available, normal gait walking motion for our biomechanical analysis in both suited and unsuited conditions. However, we recognize that walking motion in a spacesuit is different from “normal” (i.e., unsuited) walking motion.[43,44] This difference in gait is not captured in our analysis and suited results could be altered due to differences in human spacesuit-interaction. Ideally, suited gait motions should be used, for example using wearable technology that could be implemented inside the spacesuit to record true suited human motion. Future work will focus on integrating data on suited walking gaits, new xEMU joint torques, and the mass of the spacesuit. In addition, our simulations assumed the actuators performed optimally, based on the astronaut gait, using optimization algorithms built in Opensim.[45] Future work will entail approaching this problem with machine learning techniques.[31]

D. Operational Impacts on Prebreathe Time

The full-body soft-robotic layer, located inside the suit and against the body of the astronaut, also generates a certain amount of MCP. Our suit architecture allows for two potential possibilities to generate MCP. First, EPU40, the material used for the robotic actuators, has a yield strength of approximately 9 MPa and can stretch to a 300%

strain. As a result, the material could be over-pressurized and stretched to allow the astronaut to don the soft-robotic layer, then depressurized to apply a certain amount of MCP. Alternatively, the actuators could act as a restraint layer in the regions of the body that are historically difficult to apply MCP (armpits, popliteal region, etc.) and when pressurized, the actuators could expand to apply MCP against the body. We could also combine these methodologies with other existing MCP technologies.[46–49] The addition of MCP allows for: 1) a decrease in gas-pressure that results in an increase in mobility and/or b) an increase in overall pressure, which reduces pre-breathe times to avoid decompression sickness (DCS), a potentially fatal condition. When the human body transitions rapidly from a high-pressure atmosphere (e.g., the International Space Station) to a lower pressure atmosphere (e.g., EMU spacesuit), the nitrogen from body tissues gets released and forms bubbles in the bloodstream, potentially causing DCS. To prevent DCS, astronauts pre-breathe pure oxygen before EVA missions to wash out this nitrogen from the tissues in the body. The required pre-breathe time depends on multiple factors including atmospheric composition (or the atmosphere of a space station cabin), initial pressure (i.e., space station cabin), and final pressure (i.e., spacesuit). We investigated the relationship between these factors in the context of SmartSuit, including the implications of the additional MCP capability. We utilized prebreathe models based on the amount of nitrogen remaining in the tissues of the body after the pre-breathe of 100% oxygen for varying durations.[44] This model defines the following risk factor, R[44]:

$$R = \frac{P_{N_2}}{P_{Suit}} \tag{3}$$

where P_{N_2} is the partial pressure of nitrogen in the atmosphere (i.e., initial absorbed tissue N_2 pressure), P_{Suit} is the total pressure of the spacesuit, and R is the risk factor (also known as bends ratio) that evolves as a function of time during the pre-breathe of pure oxygen. The removal of nitrogen can be represented by an exponential decay curve and is dependent on the tissue half time, $t_{1/2}$, which is conventionally set to 360 minutes. Thus, R can be defined as:

$$R(t) = R(0)\exp\left[-\ln(2)\frac{t}{t_{1/2}}\right] \tag{4}$$

where $R(0)$ is the initial risk factor and $R(t)$ is the risk factor at time, t. For reference, current NASA protocols require the risk factor to be at least R = 1.6-1.7 after oxygen prebreathe.[26,50]

Figure 7 shows the relationship between spacesuit pressure, prebreathe time, and DCS risk value in three separate atmospheric conditions. Similar studies have considered the relationship between these variables but we take a more quantitative approach for each of the three variables.[51] The three atmospheres used for the analysis are the International Space Station (14.7 psia (101 kPa), 21% O_2), the Adjusted Space Shuttle (10.2 psia (70.3 kPa), 26.5 % O_2; a low pressure-high oxygen environment used before EVAs to reduce the risk of DCS), and an exploration atmosphere recommended by the Exploration Atmospheres Working Group (EAWG) based on factors such as hypoxia, flammability, mission impact, and DCS (8.2 psia (56.5 kPa), 34% O_2).[50,52] The x-axis of Figure 7 represents the total pressure of the SmartSuit spacesuit that also includes 1 psia (6.9 kPa) of MCP. For example, a total spacesuit pressure of 4.3 psia (29.6 kPa) consists of 3.3 psia (22.8 kPa) of gas pressure and 1 psia (6.9 kPa) of MCP. Similarly, a total spacesuit pressure of 5.3 psia (36.5kPa) consists of 4.3 psia (29.6 kPa) of gas pressure and 1 psia (6.9 kPa) of MCP. This range of spacesuit pressures represents the following trade off when starting with a nominal spacesuit operating pressure (4.3 psia) and either maintaining the total spacesuit pressure and reducing gas pressure by introducing MCP (i.e., 3.3 psia (22.8 kPa) gas pressure + 1 psia (6.9 kPa) MCP = 4.3 psia (29.6 kPa) total pressure) or 2) increasing the total spacesuit pressure by adding the MCP to the gas pressure (i.e., 4.3 psia (29.6 kPa) gas pressure + 1 psia (6.9 kPa) MCP = 5.3 psia (36.5kPa) total pressure). The y-axis of Figure 7 represents the calculated risk value after completing a prebreathe time indicated by the different color lines on the figures. Current operational conditions on the ISS require a 4-hour prebreathe (240 minutes) when entering a total spacesuit gas pressure of 4.3 psia (29.6 kPa) to achieve a risk value of R = 1.7. The top panel of Figure 7 confirms these calculations. For comparison, a spacesuit architecture, like that of the SmartSuit, that can apply 1 psia of MCP could benefit the astronauts by reducing the amount of prebreathe time to achieve a risk value of R = 1.7 by almost 2 hours (see top Figure 7).

The atmosphere from which the astronaut is operating plays a significant role in whether the reduction of gas pressure in the spacesuit or the increase in total pressure has greater benefit to the mission. For example, the bottom panel of Figure 7 indicates that the risk value of a 4.3 psia (29.6 kPa) spacesuit emerging from the Exploration atmosphere is already well below the R = 1.7 mark. As a result, a spacesuit with a lower gas pressure (a spacesuit environment of 3.3 psia (22.8 kPa) of gas pressure and 1 psia (6.9 kPa) of MCP) would be preferred to a spacesuit with nominal gas pressure and additional MCP due to greater benefits in mobility.

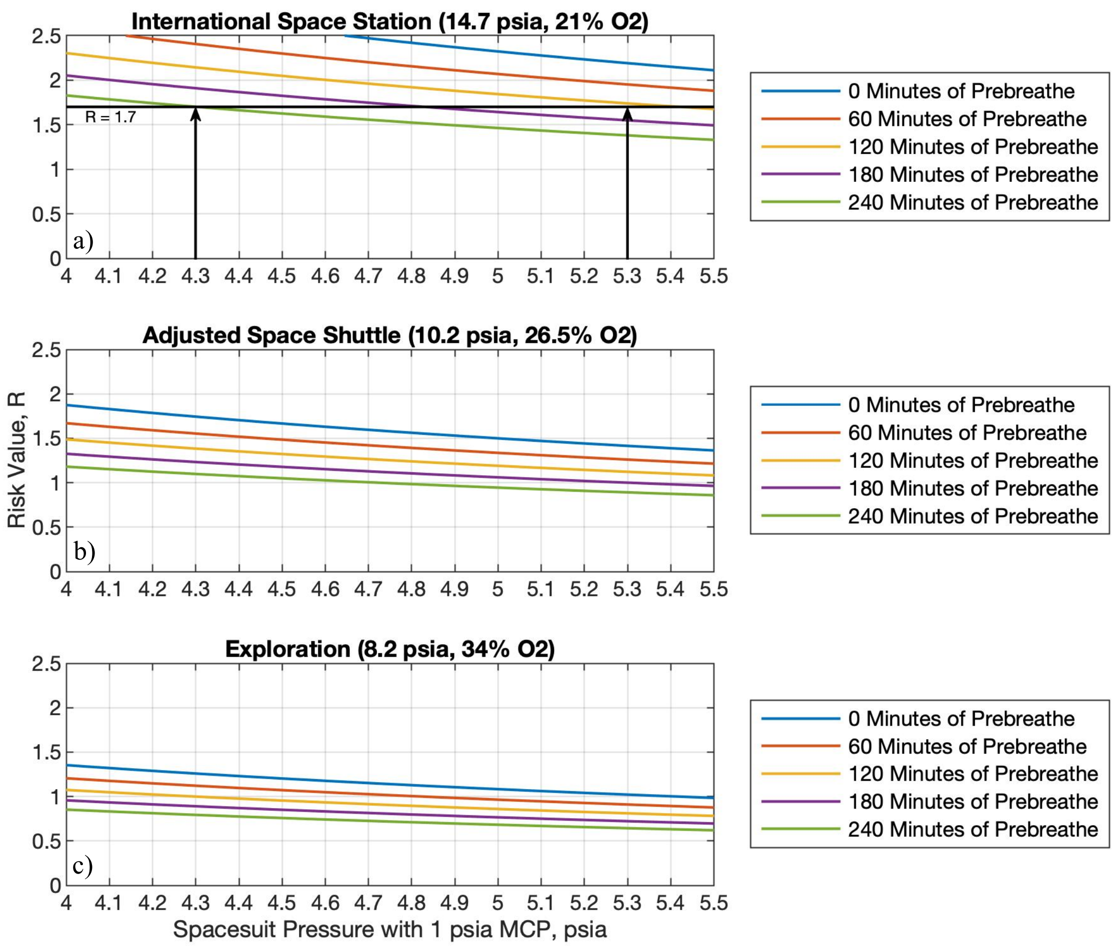

Figure 7. Trade-off between total spacesuit pressure (x-axis), prebreathe time, and risk value (y-axis) for ISS, Adjusted Space Shuttle, and Exploration atmosphere conditions. The total spacesuit pressure is a combination of gas pressure and 1 psia of MCP. For ISS conditions, the mission can benefit from increased spacesuit pressure (due to the additional MCP) as the required prebreathe time will be reduced by almost 2 hours. In comparison, there will not be operational benefits to increasing total spacesuit pressure in an environment such as the Exploration atmosphere. The risk value is already well below R = 1.7 and lower spacesuit gas pressures provide significant improvement in mobility.

There are several other factors that can be considered in the trade-off between prebreathe time, mobility, spacesuit pressure, and environmental conditions. For example, variable pressure spacesuits could take advantage of both improved mobility and reduced prebreathe times. We explore the benefits of variable pressure spacesuits and other trade-offs in the context of the SmartSuit elsewhere.[53]

III. Self-Healing Membrane

Self-healing materials can be characterized into extrinsic self-healing and intrinsic self-healing. Extrinsic self-healing materials are typically encapsulated microdroplets that can initiate polymerization once punctured. This approach is limited by the number of times it can heal. To enhance spacesuit safety, we chose an intrinsic self-healing material for the self-healable membrane, which can be cut and healed infinite times due to the mechanisms of the dynamic bonds. In addition, this material is flexible and capable of stretching to move with the astronaut. The material we developed is a self-healing polyurethane urea elastomer (sPUU), with soft segments composed of polytetramethylene glycol (PTMEG, Mw=1,000) and isophorone diisocyanate (IPDI), and a hard segment of bis (4-hydroxyphenyl) disulfide (disulfide bridge, or S-S). Self-healing is enabled primarily by the strong dynamic covalent bond of the disulfide bridge (251 kJ/mol bond energy), and partially assisted by the hydrogen bonds from the urea groups (8 kJ/mol bond energy).

To demonstrate the material's self-healing ability as a protective membrane, we made a macroscopic cut to a piece of sPUU and left it at room temperature without any intervention. Figure 8 shows the macroscopic cut mostly heals in room temperature in 1 hour and completely heals in 12 hours. As EVA usually happens in environments with extreme temperature changes, we have also characterized sPUU's working range of temperatures. A differential scanning calorimetry test shows the glass transition temperature for sPUU is -42.12°C, below which the elastomer transitions to a glassy state. Thermogravimetric analysis shows sPUU starts to decompose at 331.29°C. This working range of temperature suggests that the self-healing sensing layer should be protected by other temperature insulating layers if the EVA temperature exceeds this range.

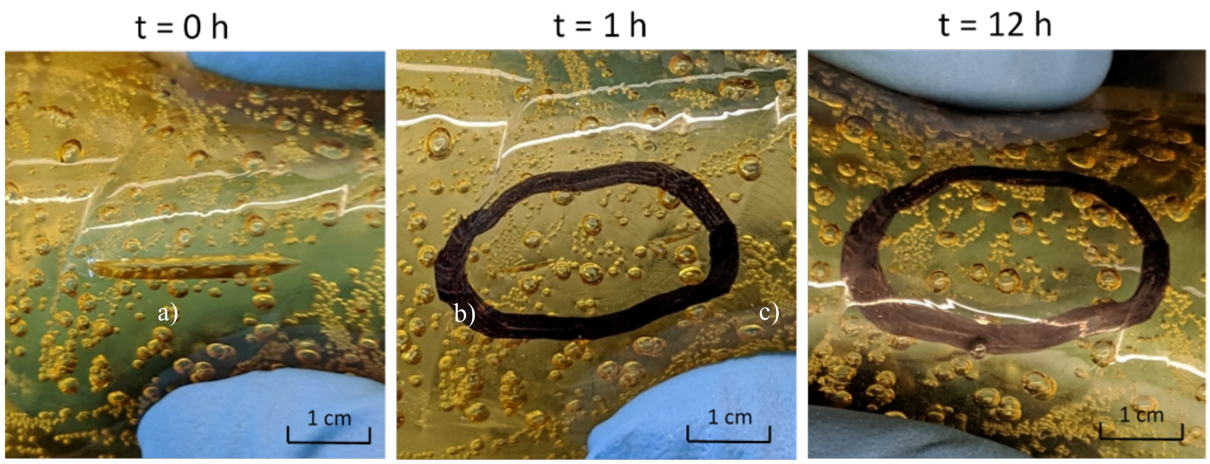

Figure 8. Macroscopic crack self-heals in room temperature. The images are shown at times t = 0 hours (a), t = 1 hour (b), and t = 12 hours (c).

IV. Stretchable Optoelectronic Sensors

In recent years, stretchable sensors for wearable applications have demonstrated their capabilities to continuously monitor health with high level of fidelity and comfort. Integrating these stretchable sensors into spacesuits could provide valuable insights into astronauts' movements during EVA. We have developed a new class of stretchable sensors based on optical waveguides, which have shown to have high sensitivity, accuracy, repeatability, and low hysteresis.[54–56] Furthermore, the optoelectronic sensors could also monitor the integrity of spacesuits for potential damage. Figure 9 demonstrates the use of an optoelectronic sensor for damage detection. These optical waveguide sensors are elastomeric waveguides made of a high refractive index core, and a low reflective index cladding. An LED is coupled to one end as the input, which is transmitted based on total internal reflection to the other end and received by a photodiode. By recording the light intensity change, deformation can be measured. Methods utilizing these sensors as wearables for human motion monitoring can be found in our previous work.[56] Furthermore, the optoelectronic sensors could also monitor the integrity of spacesuits for alert of potential damage. Figure 9 shows a stretchable waveguide made of polyurethane (Clear Flex™ 30) is embedded in a silicone matrix (SYLGARD™ 184). Deformations such as pressing cause moderate output intensity decrease; physical damages such as cuts cause temporary output intensity to decrease to zero. This is representative of a scenario in which the optoelectronic sensors are embedded in the self-healing membrane. A cut to the sensor would result in a drop in intensity but the self-healing nature of the surrounding matrix would aid in restoring the signal.

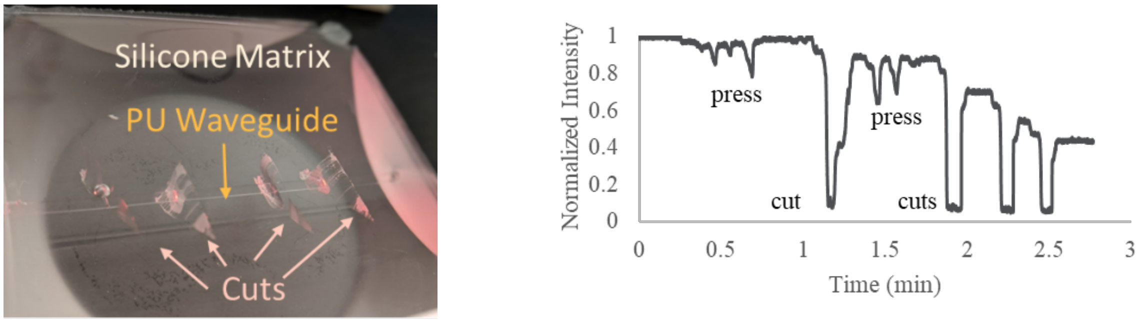

Figure 9. Damage detection with an optoelectronic sensor. Pressing down on the sensor reduces the normalized intensity perceived by the photodiode. Cutting the sensor temporarily decreases the intensity to zero.

V. Conclusion

We can apply these results into a Martian mission characterized by the Mars Design Reference Mission 5.0 (DRM 5.0).[57] If astronauts average four EVAs per week on a 539-day mission, approximately 300 EVAs would be performed per Martian stay. Traversing distances before the aid of pressurized or unpressurized rovers are estimated to be 1-2 km per EVA.[58] In addition, astronauts will walk around the work site, which we estimate to be two extra hours of walking. Assuming a gait cycle that traverses a distance of 1.4 meters in 1.2 seconds, the astronaut will be walking approximately 2 hours and 26 minutes per mission. According to our results in Table 1, the benefit from soft-robotic actuators could range from 80.5 (5 Nm actuators) to 553.9 (15 Nm actuators) kilocalories per EVA mission ((943 minus kilocalories walking with each actuator torque limit) * 2.44 hours/EVA). The safety of the EVA mission will also improve greatly due to the addition of the self-healing membrane and optoelectronic sensors. Falls during EVAs are likely, and rocks and other debris on the Martian surface may contain sharp and pointed surfaces, which can puncture the spacesuit. The SmartSuit architecture will be capable of detecting cuts or holes in the spacesuit thanks to the optoelectronic sensors. Once notified, the astronaut can affirm that the lesion has been closed by the self-healing membrane and proceed to a pressurized rover or habitat to make any necessary repairs. The combination of improved mobility and safety will greatly increase the amount of science that can be collected on every EVA mission.

Acknowledgments

We would like to acknowledge the NASA Innovative and Advanced Concepts program (grant number 80NSSC19K0969) for supporting and funding this research. We would also like to acknowledge Professor Darren Hartl and Rodney Inmon on their advice and expertise in designing and executing the actuator experiment.

References

[1]Thomas, K. S., and McMann, H. J. *U. S. Spacesuits*. Springer Science & Business Media, 2012.

[2]Opperman, R. A., Waldie, J. M. A., Natapoff, A., Newman, D. J., and Jones, J. A. “Probability of Spacesuit-Induced Fingernail Trauma Is Associated with Hand Circumference.” *Aviation, Space, and Environmental Medicine*, Vol. 81, No. 10, 2010, pp. 907–913.

[3]Opperman, R. A., Waldie, J. M., Natapoff, A., Newman, D. J., Hochstein, J., Pollonini, L., Ansari, R. R., and Jones, J. A. “Anthropometric and Blood Flow Characteristics Leading to EVA Hand Injury.” *SAE Technical Papers*, 2009.

[4]Strauss, S., Krog, R. L., and Feiveson, A. H. “Extravehicular Mobility Unit Training and Astronaut Injuries.” *Aviation, space, and environmental medicine*, Vol. 76, No. 5, 2005, pp. 469–74.

[5]Scheuring, R. A., Mathers, C. H., Jones, J. A., and Wear, M. L. “Musculoskeletal Injuries and Minor Trauma in Space: Incidence and Injury Mechanisms in U.S. Astronauts.” *Aviation, Space, and Environmental Medicine*, Vol. 80, No. 2, 2009, pp. 117–124.

[6]Strauss, S. “Extravehicular Mobility Unit Training Suit Symptom Study Report.” *NASA Technical Report*, 2004.

[7]Williams, D. R., and Johnson, B. J. “EMU Shoulder Injury Tiger Team Report.” *NASA Technical Report*, 2003.

[8]Anderson, A. P., Newman, D. J., and Welsch, R. E. “Statistical Evaluation of Causal Factors Associated with Astronaut Shoulder Injury in Space Suits.” *Aerospace Medicine and Human Performace*, Vol. 86, No. 7, 2015, pp. 606–613.

[9]Diaz, A., Anderson, A., Kracik, M., Trotti, G., Hoffman, J., and Newman, D. “Development of a Comprehensive Astronaut Spacesuit Injury Database.” *63rd International Astronautical Congress*, 2012, pp. 1–9.

[10]Newman, D. J., Anderson, A. P., Bertrand, P., Diaz, A., Hilbert, A., Hoffman, J., Kracik, M., Reyes, S., and Trotti, G. “Conclusions and Paths Forward in Space Suit Injury Countermeasures.” *NASA Human Research Program Investigator’s Workshop*, 2015.

[11]Newman, D. J., Anderson, A., Diaz, A., Kracik, M., Hilbert, A., Bertrand, P., Hoffman, J., and Trotti, G. “Spacesuit Trauma Countermeasures Research: Injury Prevention and Comfort Protection Design.” *NASA Human Research Program Investigators’ Workshop*, 2014.

[12]Hilbert, A., Diaz, A., Anderson, A. P., and Newman, D. J. “Human Spacesuit Interaction: Musculoskeletal Modeling and Statistical Analysis of Injuries.” *NASA Human Research Program Investigator’s Workshop*, 2014.

[13]Anderson, A., Diaz, A., Kracik, M., Trotti, G., Hoffman, J., and Newman, D. J. “Developing a Spacesuit Injury Countermeasure System for Extravehicular Activity: Modeling and Analysis.” *42nd International Conference on Environmental Systems*, 2012.

[14]McFarland, S., and Norcross, J. “Development of an Objective Space Suit Mobility Performance Metric Using Metabolic Cost and Functional Tasks.” *46th International Conference on Environmental Systems*, 2016.

[15]Norcross, J. R., Clowers, K. G., Clark, T., Harvill, L., Morency, R. M., Stroud, L. C., Desantis, L., Vos, J. R., and Gernhardt, M. L. “Metabolic Costs and Biomechanics of Level Ambulation in a Planetary Suit.” *NASA Technical Report*, 2010.

[16]Carr, C. E., and Newman, D. J. “Exoskeleton Energetics: Implications for Planetary Extravehicular Activity.” *IEEE Aerospace Conference*, 2017.

[17]Rader, A. A., Newman, D. J., and Carr, C. E. “Loping: A Strategy for Reduced Gravity Human Locomotion?” *37th International Conference on Environmental Systems*, 2007.

[18]Schmidt, P. B. *An Investigation of Space Suit Mobility with Applications to EVA Operations*. Massachusetts Institute of Technology. PhD Thesis, 2001.

[19]Kosmo, J. J., and Ross, A. “Space Suit Mobility Evaluations In Lunar/Mars Gravity Environments.” *Journal of Aerospace*, Vol. 107, 1998, pp. 535–542.

[20]Schmidt, P. B., Newman, D. J., and Hodgson, E. “Modeling Space Suit Mobility: Applications to Design and Operations.” *31st International Conference on Environmental Systems*, No. 01, 2001.

[21]Diaz, A., Anderson, A. P., Kracik, M., Trotti, G., and Newman, D. J. “Development of a Musculoskeletal Human Spacesuit Interaction Model.” *NASA Human Research Program Investigator’s Workshop*, 2013.

[22]Diaz, A. “Musculoskeletal Human-Spacesuit Interaction Model.” *IEEE Aerospace Conference Proceedings*, Vol. 2014-June, 2014.

[23]Fineman, R. A., McGrath, T. M., Kelty-Stephen, D. G., Andrew, A. F., and Stirling, L. A. “Objective Metrics Quantifying Fit and Performance in Spacesuit Assemblies.” *Aerospace Medicine and Human Performance*, Vol. 89, No. 11, 2018, pp. 985–995.

[24]Ross, A. “Exploration Pressure Garment.” *Joint EVA Working Group*, 2017.

[25]Belobrajdic, B., Melone, K., and Diaz-Artiles, A. Planetary Extravehicular Activity (EVA) Risk Mitigation Strategies for Long-Duration Space Missions. *npj Microgravity.* 16. Volume 7. https://doi.org/10.1038/s41526-021-00144-w.

[26]Horrigan, D., Waligora, J., Beck, B., and Trevino, R. Extravehicular Activities. In *Space Biology and Medicine* (A. Nicogossian, S. Mohler, O. Gazenko, and A. Grigoriev, eds.), American Institute of Aeronautics and Astronautics, Reston, VA.

[27]NASA. *ISS Generic Operational Flight Rules*. NSTS-12820, Vol. B, Mission Operations Directorate, NASA Johnson Space Center, Houston, TX, 2003.

[28]Conkin, J., Pollock, N. W., Natoli, M. J., Martina, S. D., Wessel, J. H., and Gernhardt, M. L. “Venous Gas Emboli and Ambulation at 4.3 Psia.” *Aerospace Medicine and Human Performance*, Vol. 88, No. 4, 2017, pp. 370–376.

[29]Conkin, J., Abercromby, A. F. J., Dervay, J. P., Feiveson, A. H., Gernhardt, M. L., Norcross, J. R., Ploutz-Snyder, R., and Wessel, J. H. “Hypobaric Decompression Sickness Treatment Model.” *Aerospace Medicine and Human Performance*, Vol. 86, No. 6, 2015, pp. 508–517.

[30]Wehner, M., Quinlivan, B., Aubin, P. M., Martinez-Villalpando, E., Baumann, M., Stirling, L., Holt, K., Wood, R., and Walsh, C. “A Lightweight Soft Exosuit for Gait Assistance.” *IEEE International Conference on Robotics and Automation*, 2013, pp. 3362–3369.

[31]Li, Z., Wang, J., Yan, S., Hao, P., Tang, P., and Dai, Y. “Research on Joint-Assisted Exoskeleton Control System of Lower Extremity in Active Spacesuit.” *International Conference on Mechatronics and Automation*, 2019.

[32]Zhao, H., Jalving, J., Huang, R., Knepper, R., Ruina, A., and Shepherd, R. “A Helping Hand: Soft Orthosis with Integrated Optical Strain Sensors and EMG Control.” *IEEE Robotics & Automation Magazine*, Vol. 23, No. 3, 2016, pp. 55–64.

[33]Diaz-Artiles, A., Shepherd, R., Kluis, L., Keller, N., Bai, H., Iyengar, N., and Audirsch, C. *SmartSuit: Hybrid, Intelligent, and Highly Mobile EVA Spacesuit for Next Generation Exploration Missions.* NASA Innovative Advanced Concepts (NIAC) - Phase I Final Report, 2020.

[34]Kluis, L., Keller, N., Bai, H., Iyengar, N., Shepherd, R., and Diaz-Artiles, A. “Reducing Metabolic Cost During Planetary Ambulation Using Robotic Actuation.” *Aerospace Medicine and Human Performance. In Press*, 2021.

[35]Delp, S. L., Anderson, F. C., Arnold, A. S., Loan, P., Habib, A., John, C. T., Guendelman, E., and Thelen, D. G. "OpenSim: Open-Source Software to Create and Analyze Dynamic Simulations of Movement." *IEEE Transactions on Biomedical Engineering*, Vol. 54, No. 11, 2007, pp. 1940–50.

[36]Anderson, F. C., and Pandy, M. G. "Dynamic Optimization of Human Walking." *Journal of Biomechanical Engineering*, Vol. 123, No. 5, 2001, p. 381.

[37]Hamner, S. R., Seth, A., and Delp, S. L. "Muscle Contributions to Propulsion and Support during Running." *Journal of Biomechanics*, Vol. 43, No. 14, 2010, pp. 2709–2716.

[38]Gilkey, A. L. *Space Suit Simulator for Partial Gravity Extravehicular Activity Experimentation and Training*. Massachusetts Institute of Technology. MS Thesis, 2012.

[39]Meyen, F. E., Holschuh, B., Kobrick, R., Jacobs, S., and Newman. "Robotic Joint Torque Testing : A Critical Tool in the Development of Pressure Suit Mobility Elements." *41st International Conference on Environmental Systems*, 2011, pp. 1–10.

[40]Umberger, B. R., Gerritsen, K. G. M., and Martin, P. E. "A Model of Human Muscle Energy Expenditure." *Computer Methods in Biomechanics and Biomedical Engineering*, Vol. 6, No. 2, 2003, pp. 99–111.

[41]Umberger, B. R. "Stance and Swing Phase Costs in Human Walking." *Journal of the Royal Society Interface*, Vol. 7, No. 50, 2010, pp. 1329–1340.

[42]Delp, S. L., Loan, J. P., Hoy, M. G., Zajac, F. E., Topp, E. L., and Rosen, J. M. "An Interactive Graphics-Based Model of the Lower Extremity to Study Orthopaedic Surgical Procedures." *IEEE Transactions on Biomedical Engineering*, Vol. 37, No. 8, 1990, pp. 757–767.

[43]Carr, C. E., and Newman, D. J. "Space Suit Bioenergetics : Framework and Analysis of Unsuited and Suited Activity." *Aviation, Space, and Environmental Medicine*, Vol. 78, No. 11, 2007, pp. 1013–1022.

[44]Carr, C. E., and McGee, J. "The Apollo Number: Space Suits, Self-Support, and the Walk-Run Transition." *PLoS ONE*, Vol. 4, No. 8, 2009.

[45]Thelen, D. G., Anderson, F. C., and Delp, S. L. "Generating Dynamic Simulations of Movement Using Computed Muscle Control." *Journal of Biomechanics*, Vol. 36, No. 3, 2003, pp. 321–328.

[46]Kothakonda, A., Kluis, L., and Newman, D. J. "System Design for Tensioning Limb Sections in a Mechanical Counter Pressure Spacesuit." *International Conference on Environmental Systems*, No. July, 2019, pp. 1–11.

[47]Southern, T. C., and Moiseev, N. A. "Novel Mechanical Counter Pressure Gloves." *International Conference on Environmental Systems*, 2017.

[48]Mody, A. A. *Proof-Of-Concept MCP Glove Prototype For The Hybrid Spacesuit Concept*. University of Colorado - Boulder. Master's Thesis, 2020.

[49]Holschuh, B. T., and Newman, D. J. "Morphing Compression Garments for Space Medicine and Extravehicular Activity Using Active Materials." *Aerospace Medicine and Human Performance*, Vol. 87, No. 2, 2016, pp. 84–92.

[50]Lange, K. E., Perka, A. T., Duffield, B. E., and Jeng, F. F. "Bounding the Spacecraft Atmosphere Design Space for Future Exploration Missions." *Nasa/Cr—2005–213689*, No. June, 2005, p. 213689.

[51]Huerta, R., Kerr, E. S., and Anderson, A. P. "Mechanical Counterpressure and Gas-Pressurized Fusion Spacesuit Concept to Enable Martian Planetary Exploration." *International Conference on Environmental Systems*, No. July, 2018.

[52]Exploration Atmospheres Working Group. "Recommendations for Exploration Spacecraft Internal Atmospheres: The Final Report of the NASA Exploration Atmospheres Working Group." *NASA Technical Report*, 2010.

[53]Kluis, L., and Diaz-Artiles, A. Revisiting Decompression Sickness Risk and Mobility in the Context of the SmartSuit, a Hybrid Planetary Spacesuit. *bioRxiv*. 2021.03.26.437246. http://biorxiv.org/content/early/2021/03/29/2021.03.26.437246.abstract.

[54]Zhao, H., O'Brien, K., Li, S., and Shepherd, R. F. "Optoelectronically Innervated Soft Prosthetic Hand via Stretchable Optical Waveguides." *Science Robotics*, Vol. 1, No. 1, 2016, p. eaai7529.

[55]Xu, P. A., Mishra, A. K., Bai, H., Aubin, C. A., Zullo, L., and Shepherd, R. F. "Optical Lace for Synthetic Afferent Neural Networks." *Science Robotics*, Vol. 4, No. 34, 2019, p. eaaw6304.

[56]Bai, H., Li, S., Barreiros, J., Tu, Y., Pollock, C. R., and Shepherd, R. F. "Stretchable Distributed Fiber-Optic Sensors." *Science*, Vol. 370, No. 6518, 2020, pp. 848–852.

[57]Mars Architecture Steering Group. "Human Exploration of Mars Design Reference Architecture 5.0." *NASA-SP-2009-566*, 2009.

[58]Alpert, B., and Johnson, B. "Extravehicular Activity Framework for Exploration - 2019." *49th International Conference on Environmental Systems*, 2019.